Highly anisotropic dispersion of surface acoustic waves in M-plane GaN layers grown on γ-$LiAlO_2(100)$

Y. Takagaki, C. Hucho, E. Wiebicke, Y. J. Sun, O. Brandt, M. Ramsteiner, and K. H. Ploog
Paul-Drude-Institut für Festkörperelektronik, Hausvogteiplatz 5-7, 10117 Berlin, Germany
(Received 20 August 2003; published 15 March 2004)

The characteristics of surface acoustic waves (SAW's) in M-plane GaN and AlN layers grown on γ-$LiAlO_2(100)$ are investigated. The SAW velocities in the (100) plane of bulk γ-$LiAlO_2$ are virtually identical along the [010] and [001] directions and are significantly larger than those in the M-plane bulk GaN. Despite these velocity relations, the SAW velocity in GaN/γ-$LiAlO_2$ heterostructures increases steadily along the GaN$[11\bar{2}0]$ direction with increasing the SAW wavelength, whereas it decreases along the GaN [0001] direction. A guided Rayleigh mode is observed solely for the propagation along the GaN$[11\bar{2}0]$ direction. These experimental results are compared with numerical simulations. Velocity bowing is indicated to govern the dispersion in the heterostructures.

DOI: 10.1103/PhysRevB.69.115317 PACS number(s): 68.35.Iv, 62.20.Dc, 68.60.Bs

I. INTRODUCTION

There has been a tremendous interest in the unique properties of the III nitrides in recent years. Their favorable optical characteristics have been crucial in commercializing light-emitting diodes and laser diodes in the blue spectral range. The large breakdown electric field and saturation velocity are also attractive for high-power and high-temperature electrical applications. Moreover, the large sound velocity and strong electromechanical coupling in AlN have been demonstrated to be suited for high-frequency acoustic devices.[1,2]

It is a natural consequence that one wishes to combine these excellent optical, electrical, and acoustic properties for creating novel devices. As a step towards this goal, we are interested in controlling the light emission due to exciton recombination by a surface acoustic wave (SAW), as demonstrated previously using GaAs by Rocke *et al.*[3] In addition, there are reports in which the electrical properties in GaAs-(Al,Ga)As resonant tunneling diodes were modulated by exposing the active region to SAW's.[4,5] These manipulations are based on the interaction between the SAW-induced piezoelectric fields and charged carriers. However, the piezoelectric fields are easily screened in GaAs when there exists a large number of free carriers in the devices because of the weak electromechanical coupling. Devices consisting of AlN and GaN may overcome this problem as the electromechanical coupling is strong in these materials.[6]

In the most extensively investigated cases of GaN and AlN layers on substrates such as $Al_2O_3(0001)$ and SiC(0001), the [0001] direction of GaN and AlN is perpendicular to the interface. This implies the problem that giant electric fields are induced along this direction due to both spontaneous and piezopolarization,[7] which quench the photoluminescence when the well width in GaN-(Al,Ga)N heterostructures exceeds about 6 nm. On the contrary, no polarization is present along the growth direction, $[1\bar{1}00]$, for M-plane GaN on a γ-$LiAlO_2(100)$ surface.[8] The M plane does not exhibit spontaneous polarization as it is nonpolar. In addition, there is no piezopolarization in strained layers as a consequence of the vanishing strain tensor components ε_{31} and ε_{32}.

In this paper, we investigate the propagation of SAW's in M-plane GaN and AlN layers grown on γ-$LiAlO_2(100)$. We examine the dispersion of Rayleigh waves in the heterostructures to extract the acoustic properties of the overlayer and the substrate. We emphasize that little is known about the elastic properties of γ-$LiAlO_2$. We provide the SAW velocities for γ-$LiAlO_2(100)$ along the [010] and [001] directions. While both of the SAW velocities turn out to be larger than those in the M plane of bulk GaN, the velocity dispersions along the [0001] and $[11\bar{2}0]$ directions of GaN layers on γ-$LiAlO_2$ are found to be surprisingly anisotropic.

II. EXPERIMENT

For the present experiments, hexagonal GaN and AlN layers were grown on tetragonal γ-$LiAlO_2(100)$ substrates by plasma-assisted molecular-beam epitaxy.[9] All samples investigated consist of pure M-plane layers as evidenced by high-resolution x-ray diffraction.[9] The crystal structure of the substrate and the orientation relationship of the epitaxial layers are illustrated in Fig. 1. The M-plane surfaces of GaN and AlN are aligned to the γ-$LiAlO_2(100)$ surface. The [0001] and $[11\bar{2}0]$ directions of GaN and AlN are parallel to the [010] and [001] directions of γ-$LiAlO_2$, respectively.

The crystal directions of γ-$LiAlO_2$ were determined by using Raman scattering. Figure 2 shows the Raman spectra in backscattering configuration $\underline{y}(u,v)\bar{y}$, where u and v denote the polarization and y and $\bar{y}$ the direction of the incident and scattered light, respectively. For each direction y, polarized ($u=v$) Raman spectra were measured with the polarization along orthogonal directions (x and z) of the γ-$LiAlO_2$ crystal: $u=v=x$ and $u=v=z$. The measurements were carried out at room temperature using a He-Ne laser for excitation at a wavelength of 632.8 nm. The c axis of γ-$LiAlO_2$ substrates is given by the direction $y=c$ for which the Raman spectra in the configurations $y(x,x)\bar{y}$ and $y(z,z)\bar{y}$ are identical. The in-plane c axis of the substrates can, therefore,

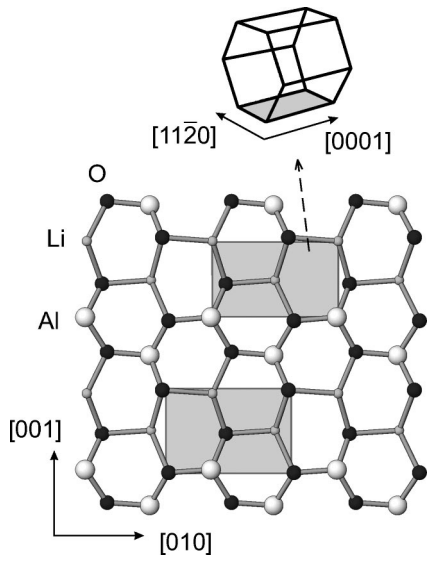

FIG. 1. Ball-and-stick model of γ-$LiAlO_2(100)$. The shaded rectangles illustrate the nucleation sites for the $(1\bar{1}00)$ plane of GaN and AlN. The $[11\bar{2}0]$ and [0001] directions of GaN and AlN are aligned along the [001] and [010] directions of γ-$LiAlO_2$, respectively.

be unambiguously determined by Raman measurements from the cleaved edges. Subsequent measurements with y perpendicular to the substrate surface, i.e., perpendicular to the c axis, revealed that, e.g., one phonon line at 610 cm^{-1} was absent in the $y(z,z)\bar{y}$ configuration when z was parallel to the c axis. The Raman spectra in Fig. 2 clearly represent the cases with the polarization perpendicular, $y(x,x)\bar{y}$, and parallel, $y(z,z)\bar{y}$ to the c axis.

Interdigital transducers (IDT's) were fabricated on the epitaxially grown surface to electrically generate SAW's. By applying a rf bias to the IDT's, SAW's are excited through the piezoelectric effect in GaN and AlN. In the device fabrication, we first prepared the contact pads of the IDT's, which

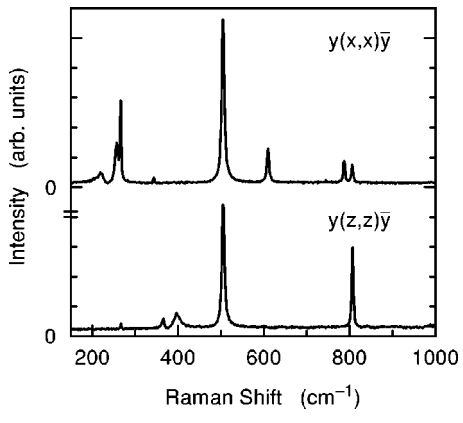

FIG. 2. Raman spectra of γ-$LiAlO_2(100)$ at room temperature. The polarized scattering configurations are $y(x,x)\bar{y}$ and $y(z,z)\bar{y}$ for the top and bottom curves, respectively. The Cartesian axes x, y, and z correspond to the [010], [100], and [001] directions, respectively. Curves are offset for clarity.

were made of a 100-nm-thick Au film, using optical lithography. Interdigitated electrodes of the transducers were defined between the pads using electron-beam lithography and the lift-off technique. A 30-nm-thick Al film that followed the deposition of a 6-nm-thick Ti film was prepared by means of electron-beam evaporation. Delay lines were constructed by aligning two nominally identical transducers along the direction of the SAW propagation. The transmission characteristics of the delay lines were evaluated using a summit-9000 analytical probe station (Cascade Microtech) with a HP 8720D network analyzer.

The transmission between the IDT's takes place not only via SAW's but also by direct electromagnetic coupling. The contribution of the direct coupling is eliminated in the transmission spectra to be presented below by exploiting the difference in the times that the signal transmission requires. The ''crosstalk'' signal is transmitted almost instantaneously at the speed of light, whereas the SAW's propagate at the sound velocity. By Fourier transforming a raw transmission spectrum, the impulse response of a delay line can be simulated. The crosstalk and the SAW transmission can be isolated from each other by selecting the corresponding component in the time domain. This technique enables us to determine the SAW frequency even if the SAW transmission is significantly weak.

III. SAW CHARACTERISTICS IN SUBSTRATES

In this section, we experimentally investigate the characteristics of SAW's propagating on the surface of bulk γ-$LiAlO_2$. It turns out that SAW's can be excited directly in γ-$LiAlO_2$ by preparing IDTs on its surface. As γ-$LiAlO_2$ reacts fairly strongly with acids and alkalis, i.e., typical developers of photoresists, the IDT's were fabricated using electron-beam lithography instead of optical lithography. However, γ-$LiAlO_2$ is an insulator, and so multiple layers consisting of polymethylmethacrylate (PMMA), polyimide, and a sheet of Au were employed for the lithography and lift-off process. The pattern delineated in PMMA was transferred to polyimide by ozone etching. γ-$LiAlO_2$ is reactive to ozone, and so its surface was slightly corrugated despite the sophisticated fabrication method.

We aligned delay lines along the [010], [001], and [011] directions on the (100) surface. The SAW wavelength was $\lambda_s \approx 3.7$ μm. The aperture and the length of the IDT's were 0.3 and 0.5 mm, respectively. The center-to-center distance between the IDT's was 1.5 mm.

In Fig. 3, we plot the SAW transmission amplitude against the velocity calculated using the frequency f and λ_s. The SAW velocities are obtained to be $v_s = 5.0$ km/s in both the [010] and [001] directions. The virtually identical v_s in the directions perpendicular and parallel to the c axis of γ-$LiAlO_2$ is an unexpected coincidence. The spectra exhibit additional small peaks in $fv_s \leqslant 4.6$ km/s. We consider these peaks spurious as their existence and the position in the velocity vary among nominally identical samples. Corrugations are generally produced on the γ-$LiAlO_2$ surface underneath the interdigitated gate electrodes because of the material's reactivity to ozone, which was used in the fabrication of the

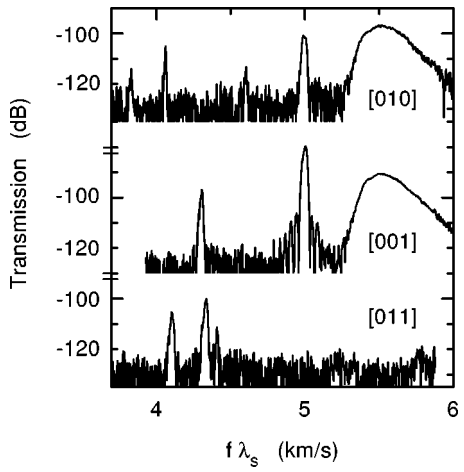

FIG. 3. Transmission spectra of delay lines with IDT's having a SAW wavelength $\lambda_s \approx 3.7$ μm prepared directly on γ-$LiAlO_2(100)$. Rayleigh-wave excitation takes place at $f\lambda_s = 5.0$ km/s, with f being the frequency, along both the [010] and [001] directions. The excitation is absent when the delay line is set along the [011] direction. The broad peak at $f\lambda_s \sim 5.5$ km/s is ascribed to bulk-wave excitation.

IDT's. The spurious peaks may originate from multiple scattering of SAW's within the IDT's.

We deduce following speculations about the electromechanical coupling in γ-$LiAlO_2$ based on the transmitted SAW amplitude. Although the nature of the SAW's, including beam spreading and steering effects and the attenuation during the propagation, has to be assessed for a reliable evaluation, we neglect all of these in the following qualitative arguments because of the relatively small SAW propagation distance between the IDT's. First, the electromechanical coupling is suggested to be stronger along the [001] direction than along the [010] direction. Second, when identical delay lines were patterned on the (100) surface of GaAs for [011] propagation, the insertion loss was -20 dB. This may suggest that the electromechanical coupling coefficient of γ-$LiAlO_2$ is substantially smaller than that (0.06%) of GaAs. Third, the Rayleigh-wave excitation is absent when the delay line is prepared along the [011] direction, suggesting that the electromechanical coupling is negligibly small along this direction. We will return to this point later.

IV. SAW CHARACTERISTICS IN HETEROSTRUCTURES

We turn our attention to the properties of the SAW's in GaN/γ-$LiAlO_2$ heterostructures. In Fig. 4, we show the transmission spectra of delay lines having $\lambda_s = 1.2$ μm. The delay lines were fabricated on a GaN layer of thickness $d = 700$ nm. The inset of Fig. 4 shows an atomic-force-microscope image of the surface of this GaN layer. Epitaxial GaN and AlN layers exhibit a characteristic ''slate-like'' morphology with stripes elongated along the $[11\bar{2}0]$ direction.[10–12] The root-mean-square magnitude of the height modulation is merely 0.6 nm for the GaN layers under investigation. The roughness is thus insignificant for SAW propagation.

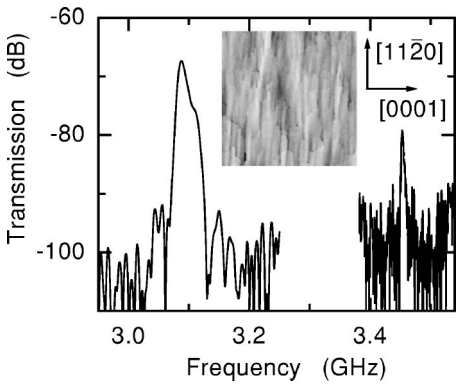

FIG. 4. Transmission spectra of the delay lines prepared on a 700-nm-thick GaN layer grown on a γ-$LiAlO_2(100)$ substrate. The SAW wavelength is $\lambda_s = 1.2$ μm. The directions of the SAW propagation for the curves in the left- and right-hand sides are along the [0001] and $[11\bar{2}0]$ directions of GaN, respectively. The inset shows a surface image of the GaN layer obtained by atomic force microscope. The scan area is 3×3 μm^2. The peak-to-valley and root-mean-square magnitudes of the height modulation are 6.5 and 0.6 nm, respectively.

The two curves in Fig. 4 are associated with the SAW propagation along the [0001] (left-hand side) and $[11\bar{2}0]$ (right-hand side) directions of GaN. The piezoelectricity of GaN and AlN occurs along the c axis, presumably accounting for the significantly larger SAW transmission amplitude along the GaN[0001] direction than along the GaN$[11\bar{2}0]$ direction. Despite the large electromechanical coupling in GaN,[6] the transmission amplitude is small. We attribute this to the large background carrier density (1×10^{24} m^{-3}) in the as-grown M-plane GaN layers. The electrons screen the rf voltage and hence suppress the SAW generation. The quenching of the piezoelectric fields by the electrons also disrupts the SAW detection. The free carriers were found to be not too problematic in GaN layers grown on SiC substrates.[6] However, this may no longer be the case for the GaN layers grown on γ-$LiAlO_2$ as the carrier density is about an order of magnitude larger there in comparison to that in the GaN layers on SiC.[13]

In Figs. 5(a) and 5(b), we plot (symbols) v_s for various values of λ_s for the SAW propagation directions of GaN $[11\bar{2}0]$ and GaN[0001], respectively. When the SAW propagation is set to be along the GaN[0001] direction, v_s decreases with an increase of λ_s. For $2.0 < \lambda_s < 4.5$ μm, v_s appears to be roughly independent of λ_s. On the contrary, the SAW propagation becomes monotonously faster for larger λ_s in the GaN$[11\bar{2}0]$ direction. In the limit of large λ_s, v_s should be given by the SAW velocity in the substrate. The velocity-saturation regime is not reached when $d/\lambda_s = 0.16$. We are hence unable to determine the SAW velocity in γ-$LiAlO_2$ from the SAW dispersion in the heterostructures.

An acoustic wave is confined in the overlayer when the sound velocity in the substrate exceeds that in the overlayer. As a consequence, guided Rayleigh modes emerge roughly when λ_s is less than d.[6] As anticipated from the steady in-

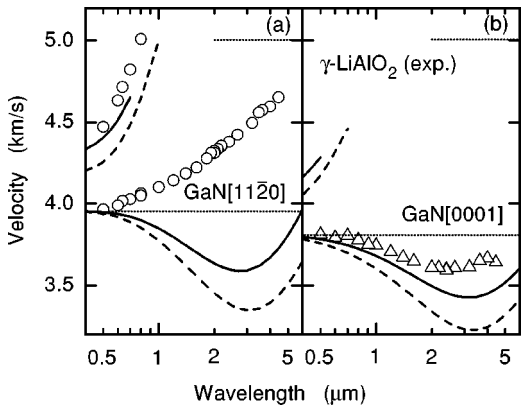

FIG. 5. Dependence of the SAW velocity v_s on the SAW wavelength λ_s. The direction of SAW propagation is (a) perpendicular to the c axis of GaN (along the γ-$LiAlO_2[001]$ direction) and (b) along the c axis of GaN (along the γ-$LiAlO_2[010]$ direction). The structure consists of a 700-nm-thick GaN layer grown on γ-$LiAlO_2(100)$. The solid and dashed lines show numerical predictions of the dispersion when c_{44} and c_{66} are 0.7 and 1.5 $\times 10^{11}$ N/m^2, respectively. The dotted lines indicate v_s on the surfaces of bulk GaN (theoretical) and γ-$LiAlO_2$ (experimental).

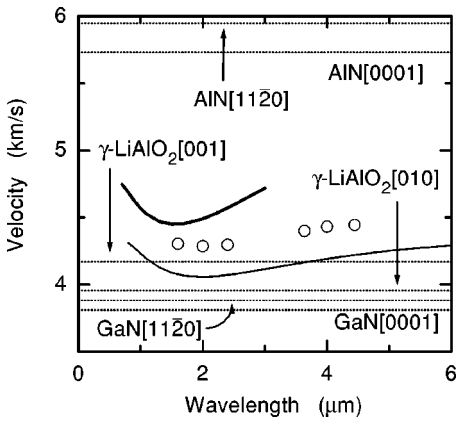

FIG. 6. Dependence of the SAW velocity v_s on the SAW wavelength λ_s. The structure consists of a 225-nm-thick AlN layer grown on a 85-nm-thick GaN buffer layer on γ-$LiAlO_2(100)$. The direction of the SAW propagation is perpendicular to the c axis of GaN (along the [001] direction of γ-$LiAlO_2$). Numerical predictions are shown by the solid lines. The elastic constants c_{44} and c_{66} of γ-$LiAlO_2$ are assumed to be 0.7×10^{11} N/m^2. The thick and thin lines correspond to the SAW propagation along the [11$\bar{2}$0] and [0001] directions of GaN, respectively. The dotted lines indicate v_s on the surfaces of bulk crystals.

crease of v_s with λ_s, the guided mode is indeed observed along the GaN[11$\bar{2}$0] direction for $\lambda_s \leqslant 0.8$ μm. The velocity of the guided mode decreases rapidly with decreasing λ_s. The guided mode is not detected along the GaN[0001] direction. The absence of the guided mode together with the decrease of v_s when λ_s is increased could be interpreted to mean that SAW's propagate slower in the substrate than in the overlayer along the GaN[0001] direction. This velocity relation would lead to a unidirectional confinement of SAW modes. However, v_s in γ-$LiAlO_2$ evaluated in the preceding section indicates that this is not the case.

In utilizing the optical and electrical properties of GaN, GaN-(Al,Ga)N quantum wells are likely to be employed to confine carriers. We have, therefore, investigated the SAW dispersion also in an AlN/GaN/γ-$LiAlO_2$ heterostructure. The thicknesses of the AlN and GaN layers were 225 and 85 nm, respectively. In Fig. 6, we show the λ_s-dependence of v_s. Due to quasiregular cracks in the epitaxial layer that run in the [11$\bar{2}$0] direction of AlN and GaN, the SAW propagation was allowed in this particular sample only along this direction. The cracks occurred because of the tensile strain in the AlN layer with respect to the GaN buffer layer. As SAW's propagate faster in AlN than in GaN,[6] v_s exhibits a minimum at $\lambda_s \approx 2$ μm.

V. DISCUSSION

In the limit of $\lambda_s \to 0$, v_s in layered structures approaches the value in the overlayer. Therefore, the in-plane anisotropy of v_s in the directions perpendicular and parallel to the c axis is indicated to be fairly small both in the GaN(1$\bar{1}$00) and γ-$LiAlO_2(100)$ surfaces in comparison to the difference of v_s between the two materials. However, the SAW dispersion exhibits dramatic anisotropy when the two materials are stacked. In order to try to understand, in particular, the reduction of v_s for large λ_s along the GaN[0001] direction, we have numerically estimated the SAW velocities.

Let us consider the (100) surface of either a tetragonal or hexagonal crystal. Since the piezoelectric constants of γ-$LiAlO_2$ are unknown, we neglect the piezoelectric coupling throughout our calculations. This assumption is justified as the electromechanical coupling appears to be weak in γ-$LiAlO_2$. The displacement vector **u** of particles of the medium obeys the following wave equation:

$$c_{ijkl}\frac{\partial^2 u_k}{\partial x_l\,\partial x_i}=\rho\frac{\partial^2 u_j}{\partial t^2}, \tag{1}$$

where c_{ijkl} is the elastic tensor and ρ is the mass density. For the x propagation on the z surface, a Rayleigh-type surface wave with the wave number $q=\omega/v_s$ and the angular frequency $\omega=2\pi f_s$ is described as

$$\begin{pmatrix} u_x \\ u_z \end{pmatrix} \propto \begin{pmatrix} 1 \\ i\gamma \end{pmatrix} e^{-q\Omega z} e^{i(qx-\omega t)}, \tag{2}$$

where Ω is a solution of

$$(\rho v_s^2 - c_1 + c_{11}\Omega^2)(\rho v_s^2 - c_2 + c_1\Omega^2) + (c_1+c_3)^2 = 0 \tag{3}$$

and

$$\gamma = \frac{(c_1+c_3)\Omega}{\rho v_s^2 - c_1 + c_{11}\Omega^2}. \tag{4}$$

The coefficients c_1, c_2, and c_3, which are listed in Table I, depend on the direction of SAW propagation. For a bulk crystal, the stress-free condition $c_{izkl}\partial u_k/\partial x_l = 0$ at the surface $z=0$ leads to the following relation:

TABLE I. Coefficients c_1, c_2, and c_3 for the [010] and [001] propagations of surface waves. The coefficients are identical for the (100) surfaces of tetragonal and hexagonal crystals.

	c_1	c_2	c_3
[010] propagation	c_{66}	c_{11}	c_{12}
[001] propagation	c_{44}	c_{33}	c_{13}

$$\mathrm{Im}[(\gamma+\Omega)^*(c_3-c_{11}\gamma\Omega)]=0. \quad (5)$$

In our simulations, we calculate Ω from Eq. (3) for a given value of v_s. The value of v_s that satisfies Eq. (5) corresponds to the SAW velocity. In layered structures, the continuity conditions for **u** at the interfaces are additionally imposed to determine v_s. The material parameters that we used in our simulations are summarized in Table II. The experimentally determined lattice constants, 5.1687 and 6.2679 Å, respectively, for perpendicular and parallel to the c axis, were used to estimate ρ of γ-$LiAlO_2$. Among the elastic constants of γ-$LiAlO_2$, c_{11}, c_{12}, c_{13}, and c_{33} were measured experimentally using a pulse-echo method. Details of this measurement will be published elsewhere. We note that the two solutions of Ω^2 obtained from Eq. (3), Ω_1^2 and Ω_2^2, are real for bulk GaN and AlN, whereas they are complex conjugate for bulk γ-$LiAlO_2$.

The remaining elastic constants c_{44} and c_{66} of γ-$LiAlO_2$ are unknown. We first attempted to determine these elastic constants by fitting v_s of bulk γ-$LiAlO_2$ to experimental values. As one finds in Table I, c_{44} and c_{66} can be estimated separately from v_s in the [001] and [010] directions, respectively. However, numerically calculated v_s of γ-$LiAlO_2$ was considerably less than the experimental values of $\approx$5.0 km/s for any values of c_{44} and c_{66}.

We have, therefore, calculated the dispersion in the layered system for a number of values of c_{44} and c_{66} in order to, at least, understand qualitatively the anomalous anisotropy. The solid and dashed lines in Fig. 5 show numerically predicted v_s-λ_s relations when c_{44} and c_{66} are 0.7 and 1.5 $\times 10^{11}$ N/m^2, respectively. In bulk γ-$LiAlO_2$, v_s in the [001] and [010] direction is, respectively, 4.168 (4.606) and 3.883 (4.174) km/s when c_{44} and c_{66} are 0.7 (1.5)$\times 10^{11}$ N/m^2. The dispersion curves are practically indistinguishable when c_{44} and c_{66} are between 0.5 and 0.8$\times 10^{11}$ N/m^2. SAW modes do not exist when c_{44} and c_{66} are less than 0.5 $\times 10^{11}$ N/m^2.

TABLE II. Mass density ρ (in units of 10^3 kg/m^3) and elastic constants c_{ij} (in units of 10^{11} N/m^2) of GaN, AlN, and γ-$LiAlO_2$. The elastic constants of γ-$LiAlO_2$ were measured by a pulse-echo method.

	ρ	c_{11}	c_{12}	c_{13}	c_{33}	c_{44}	c_{66}
GaN	6.15	3.7	1.45	1.1	3.9	0.98	1.125
AlN	3.23	4.1	1.4	1	3.9	1.2	1.35
γ-$LiAlO_2$	2.64	1.18	0.585	0.602	1.495		

The agreement between the numerical and experimental results is not satisfactory, apart from the small-λ_s regime, for which v_s is dominated by the elastic properties of GaN. The relatively good agreement obtained for the guided mode is due to its confinement in the GaN overlayer. Nevertheless, the numerical results point out an important characteristic of the SAW's in the GaN/γ-$LiAlO_2$ heterostructures. The simulation predicts that v_s decreases initially when λ_s is increased. This velocity-bowing behavior is presumably responsible for the velocity reduction with increasing λ_s along the GaN[0001] direction. However, the simulation expects a bowing effect also along the GaN[$11\bar{2}0$] direction comparable with that along the GaN[0001] direction. This is the opposite behavior compared to that observed experimentally.

Since the SAW dispersions in GaN layers grown on Al_2O_3 (Ref. 14) and SiC (Ref. 6) generally show good agreement with numerical results, we attribute the discrepancies to the uncertainties of the properties of γ-$LiAlO_2$. To begin with, the SAW excitation direction observed in Fig. 3 is surprising. It can be shown, see the Appendix, that the electromechanical coupling for this case is absent in the [010] and [001] directions, similar to the case in GaAs. The absence of the SAW excitation in the [011] direction in Fig. 3 is again in contradiction with theoretical expectation, unless the SAW's attenuate strongly along this direction. Clarifying the origin of this unexpected behavior will lead us to understand the anisotropy of the SAW dispersion.

The disagreement between the experiment and the theory might originate from the fact that γ-$LiAlO_2$ changes to α phase (trigonal structure) under intense electron-beam irradiation.[15] However, we do not think that the electron-beam-induced phase transition is relevant in our experiments as both the acceleration voltage (15 kV) and the dose were small in the electron-beam lithography. A possible explanation may be a coupling of the Rayleigh modes to transverse displacements.[14] The unknown elastic constants of γ-$LiAlO_2$, c_{44} and c_{66}, have to be determined to examine this possibility.

The numerically derived dispersion curves in AlN/GaN/γ-$LiAlO_2$ heterostructures are shown by the solid lines in Fig. 6. Here, we have assumed $c_{44}=c_{66}=0.7\times 10^{11}$ N/m^2 for γ-$LiAlO_2$. Although the simulation reproduces the variation of v_s with λ_s reasonably well, the quantitative agreement of v_s is rather poor. It ought to be pointed out that the overestimate of v_s may suggest that the ratio of the AlN and GaN layer thicknesses is less than that assumed in the calculation.

Finally, we note that Gulyaev-Bleustein waves are known to exist when the c axis of hexagonal crystals lies in the plane of the surface.[16] For these waves, the nonzero displacement is only along the c axis and the propagation direction is perpendicular to the c axis. Therefore, such waves, in principle, are not excited by the IDT's. However, Gulyaev-Bleustein waves may play a role in the SAW transmission spectra if Rayleigh waves are scattered into them, for instance, by cracks in the epitaxial layers.

VI. CONCLUSION

In conclusion, we have investigated the acoustic properties in GaN/γ-$LiAlO_2$ heterostructures by measuring v_s for

various values of λ_s. The SAW velocities in the (100) surface of γ-$LiAlO_2$ along the [010] and [001] directions are found to be virtually identical at 5.0 km/s. The SAW velocities in the M plane of GaN along and perpendicular to the *c* axis are estimated to be 3.8 and 4.0 km/s, respectively. Despite the fact that v_s in γ-$LiAlO_2$ is considerably larger than that in GaN, v_s in GaN/γ-$LiAlO_2$ heterostructures decreases along the GaN[0001] direction when λ_s is increased. Numerical calculations indicate that the velocity-bowing effect is responsible for the anomalous dispersion.

ACKNOWLEDGMENTS

We would like to thank A. Schönrock for the assistance in the sample processing. This work was supported in part by the Deutsche Forschungsgemeinschaft and by the NEDO collaboration program.

APPENDIX: ELECTROMECHANICAL COUPLING

We show that the electromechanical coupling coefficients for the SAW's propagating in the [010] and [001] directions on the (100) surface of γ-$LiAlO_2$ are zero.

The wave equations that govern piezoelectric SAW's are

$$c_{ijkl}\frac{\partial^2 u_k}{\partial x_l\,\partial x_i}+e_{kij}\frac{\partial^2 \phi}{\partial x_k\,\partial x_i}=\rho\frac{\partial^2 u_j}{\partial t^2} \tag{A1}$$

$$e_{ikl}\frac{\partial^2 u_k}{\partial x_l\,\partial x_i}-\epsilon_{ik}\frac{\partial^2 \phi}{\partial x_k\,\partial x_i}=0, \tag{A2}$$

where e_{kij} is the piezoelectricity tensor and ϵ_{ik} is the electric permittivity tensor.

The nonzero piezoelectricity components of γ-$LiAlO_2$ are $e_{14}=-e_{25}$ since it belongs to 422 symmetry class. For the Rayleigh mode propagating in the [010] direction on the (100) surface, the wave equations reduce to

$$\begin{bmatrix} \rho v_s^2+c_{11}\Omega^2-c_{66} & -i\Omega(c_{12}+c_{66}) & 0 \\ -i\Omega(c_{12}+c_{66}) & \rho v_s^2+c_{66}\Omega^2-c_{11} & 0 \\ 0 & 0 & \epsilon(1-\Omega^2) \end{bmatrix} \times\begin{pmatrix} u_{x0} \\ u_{y0} \\ \phi_0 \end{pmatrix}=\begin{pmatrix} 0 \\ 0 \\ 0 \end{pmatrix}. \tag{A3}$$

All terms involving e_{kij} vanish, and so the piezoelectricity is decoupled from the surface wave. As the SAW velocities for free and shorted surface conditions are, as a consequence, identical, the electromechanical coupling is absent. The absence of the electromechanical coupling is concluded also for the [001] direction on the (100) surface. This situation is similar to the zero electromechanical coupling for the [100] propagation on the (001) surface of GaAs, for which nonzero piezoelectricity components are $e_{14}=e_{25}=e_{36}$. Similarly, it can be shown that the electromechanical coupling is finite when the SAW propagation direction is [011].

[1] Y. Takagaki, P.V. Santos, E. Wiebicke, O. Brandt, H.-P. Schönherr, and K.H. Ploog, Appl. Phys. Lett. **81**, 2538 (2002).
[2] Y. Takagaki, O. Brandt, and K.H. Ploog, Jpn. J. Appl. Phys., Part 1 **42**, 1594 (2003).
[3] C. Rocke, S. Zimmermann, A. Wixforth, J.P. Kotthaus, G. Böhm, and G. Weimann, Phys. Rev. Lett. **78**, 4099 (1997).
[4] V.I. Talyanskii, A.B. Hutchinson, I.E. Batov, D.A. Ritchie, and E.H. Linfield, J. Appl. Phys. **86**, 2917 (1999).
[5] A.B. Hutchinson, V.I. Talyanskii, M. Pepper, G. Gumbs, G.R. Aizin, D.A. Ritchie, and E.H. Linfield, Phys. Rev. B **62**, 6948 (2000).
[6] Y. Takagaki, P.V. Santos, E. Wiebicke, O. Brandt, H.-P. Schönherr, and K.H. Ploog, Phys. Rev. B **66**, 155439 (2002).
[7] F. Bernardini and V. Fiorentini, Phys. Rev. B **56**, 10 024 (1997).
[8] P. Waltereit, O. Brandt, A. Trampert, H.T. Grahn, J. Menniger, M. Ramsteiner, M. Reiche, and K.H. Ploog, Nature (London) **406**, 865 (2000).
[9] Y.J. Sun, O. Brandt, and K.H. Ploog, J. Vac. Sci. Technol. B **21**, 1350 (2003).
[10] P. Waltereit, O. Brandt, M. Ramsteiner, K.H. Ploog, R. Uecker, and P. Reiche, J. Cryst. Growth **218**, 143 (2000).
[11] C.Q. Chen, M.E. Gaevski, W.H. Sun, E. Kuokstis, J.P. Zhang, R.S.Q. Fareed, H.M. Wang, J.W. Yang, G. Simin, M.A. Khan, H.-P. Maruska, D.W. Hill, M.M.C. Chou, and B. Chai, Appl. Phys. Lett. **81**, 3194 (2002).
[12] C.D. Lee, R.M. Feenstra, J.E. Northrup, L. Lymperakis, and J. Neugebauer, Appl. Phys. Lett. **82**, 1793 (2003).
[13] Y.J. Sun, O. Brandt, B. Jenichen, and K.H. Ploog, Appl. Phys. Lett. **83**, 5178 (2003).
[14] K.H. Choi, H.J. Kim, S.J. Chung, J.Y. Kim, T.K. Lee, and Y.J. Kim, J. Mater. Res. **18**, 1157 (2003).
[15] T.Y. Liu and A. Trampert (private communication).
[16] S.V. Biryukov, Y.V. Gulyaev, V.V. Krylov, and V.P. Plessky, *Surface Acoustic Waves in Inhomogeneous Media* (Springer, Berlin, 1995), Chap. 1.2.